Answers to review comments CBM-TRD

We would like to express our thanks to the members of the internal review committee for the careful and competent evaluation of the project and the technical design report. The comments and suggestions were very helpful in improving the overall detector design and sharpening the description of the project. Below we try to answer the specific comments raised by the committee members.

Cavern access and reliability

When discussing aspects of failure modes and reliability of detector elements and systems, the difference of detector accessibility between ALICE and CBM was pointed out in order to argue for less stringent requirements. The reviewers do strongly discourage the CBM collaboration to think along such lines.

The CBM detector is a large-scale installation that does not allow easy access to all elements. Moving detector structures to access subsystems will pose some risk of damage to other systems, it will cause detector misalignment etc., so it is evident that such interventions would only be decided in case of serious performance degradation, which will already affect the data quality. Data sets with different quality, acceptance, etc. are difficult to combine into a coherent analysis, so this situation clearly has to be avoided from the outset.

Concerning the overall operation, a loss of beam time due to frequent needs for access is clearly connected with a loss of physics operation time and issues of quality and many access requests can quickly lead to a significant degradation of scientific output.

The reviewers therefore encourage the CBM-TRD collaboration to make the minimization of access requirements a central requirement for the overall detector concept and ensure reliable operation of the system by stringent QA, robust solutions and by avoiding single point failures. In many cases this is not necessarily a cost driver, but it is more a question of a proper engineering effort.

We certainly agree with the referees on this point. Generally, the operation scheme of CBM will be such that there are no interventions foreseen during a run in order not to waste data taking time. Thus, it is for the TRD, as for any other detector system in CBM, mandatory to guarantee a stable and fail safe operation. For the TRD we aim to achieve this goal by making use of simple and robust technological solutions. E.g. the construction of the MWPCs follows a well-established concept and has proven to be reliable during operation (e.g. test beams and the similar design adopted in the ALICE-TRD). Also, the TRD will be constructed in a very modular way, i.e. every TRD module is in principle an independent entity and can be switched off during data taking without affecting the operation of the rest of the detector. Also, this modularity will allow to for an quick and easy replacement of any module by a spare during relatively short shutdown periods.
Before final installation, it is essential to perform rigorous QA tests on all levels of the system (ASICs, front-end board, readout chambers, full detector layer) in order to keep the failure rate as low as possible during data taking. We tried to emphasize throughout the technical design report the measures and precautions taken to ensure a reliable operation and also to discuss those aspects of the detector design which might be critical in this respect (single point of failures) and what consequences might arise. In addition, the mCBM-demonstrator setup will include four fully equipped TRD modules, which can extensively be tested in a realistic data-taking scenario. This will allow to ensure that the final TRD design is operating according to its specifications.

Modifications:
We tried to take this comment into account in all relevant parts of the revised TDR text.

Physics discussion

The TDR describes rather detailed studies of the physics performance for observables, which would profit from the presence of a TRD. These include the detection of a thermal dielectron signal in the Intermediate Mass Region (IMR), the study of J/psi production in p-A collisions, and the detection/identification of nuclear fragments.

For the first two items, a discussion of the respective merits of the dielectron vs. dimuon channel is somewhat missing. Since the most accurate data collected up to now on thermal dilepton production have come from a dimuon experiment (NA60 at CERN-SPS), it would be useful if the Collaboration could discuss in some detail the specific advantages of a dielectron measurement for this observable, which represents, in our opinion, the flagship measurement for the CBM-TRD.

This point is now discussed in detail in the new section 3.1.1. The main reason for following two approaches within CBM is that it is important to have a cross check of the physics results by two independent measurements with different systematics. In addition, the performance in the dimuon channel will degrade towards lower energies, since the absorber thickness will have to be thinner and due to the higher contribution from weak decays of hadrons the trigger will be less efficient. The performance of measurements in the dielectron channel on the other side should to first order be independent of the beam energy and also provide a larger acceptance towards low p_t at mid-rapidity.

Modifications:
Addition of a new subsection 3.1.1

Concerning the results of the physics performance study for intermediate mass dileptons, it would be good if the study of the invariant mass could be extended up to ~3 GeV/c^2 (now studies run out of statistics at ~2 GeV/c^2). Since the TRD becomes crucial for electron ID for p>8 GeV/c, we expect the region beyond 2 GeV/c^2 to be the one where the benefits of such a detector becomes more appreciable.

Within the current simulation framework is will be very difficult to extend the dilepton simulations towards higher masses, since the yield drops exponentially with invariant mass and the required CPU time would be excessive. An alternative to the current simulation scheme, which is based on a detailed simulation of the detector response, would be a fast simulation framework, which employs simplified parameterizations of the detector response and thus would allow to generate more statistics within the same time. However, this approach still needs to be developed and tested and is thus not available in the timeframe of the technical design report. However, for the argumentation in chapter 3 we believe it is also not really necessary to extend the spectra to higher masses. Without a TRD in the CBM setup, the signal-to-background ratio will be prohibitively low in the mass region between 1.0 – 2.0 GeV/c^2 (see, e.g., the right panel of Fig. 3.4), while with a four layer TRD the background can be suppressed to a minimal level. For the extraction of the inverse slope parameters only the mass range between 1.5 – 2.5 GeV/c^2 is relevant, anyway, so we believe that from this point of view there is also no necessity to extend the simulations.

Connected with this observation, it is shown, when discussing the origin of the combinatorial background, the breakdown in e-e, e-pi, pi-pi. Up to 2 GeV/c^2, this background, which accounts for 99% of the measured yield, looks dominated from e-e rather than from misidentified pions. One might even wonder if there is a real necessity, for this measurement in the IMR, to have the pion rejection factor ensured by 4 TRD planes. It would be good if it could be shown what happens with just 3 or 2 TRD planes, to evaluate the necessity of having 4 as in the current design.

We now show a comparative study of the detector layouts with 3, 4 and 5 layers (see Figs. 3.5, 3.6 and 3.7). All these simulation have been preformed with the new optimized geometry, which is now described in the TDR. While going to five layers does not improve the signal-to-background ratios in comparison to four layers beyond the e-e contribution, as already discussed in the first

TDR draft, the three-layer scenario is clearly worse. As shown in Fig. 3.6, the background components containing misidentified hadrons (i.e. e-pi and p-X) reach the same level than the irreducible e-e component already for invariant masses around 1.5 GeV/c^2 (for four and five layers it is still significantly lower up to masses above 2.0 GeV/c^2). This is also summarized in the new Fig. 3.7, which shows the S/B-ratios in different mass ranges (omega, phi and thermal region). Except for the omega-region, the relevant e-pi component changes visibly between three and four layers, while it remains essentially constant between four and five layers. Thus, we conclude that four layers offer a significant gain in physics performance over three layers, while adding a fifth layer does not improve the situation any further.

Modifications:
Revision of Figs. 3.4, 3.5 and 3.6
Addition of Fig. 3.7 and Tab. 3.2
Revision of text in Sects. 3.2.4 and 3.2.5

Possibly, also the other observables mentioned (J/psi production in p-A, identification of fragments) would be feasible with a smaller number of detector planes.

We have performed an additional study on the fragment identification with different number of detector layers (i.e. 3, 4 and 5 layers). Naturally, the resolution continuously improves by adding more and more layers to the setup. Already with three layers it would in principle be sufficient for a good separation of d and ^{4}He. However, four layers provide an additional safety margin and provide the additional option of calculating a truncated mean energy loss, which results in less tail-dominated dE/dx-distributions.
As the J/ψ is an observable that does not directly determine the performance requirements we did not do any studies here yet (mainly, also due to manpower reasons). In p-A the background is not such a dominant issue than in A+A, so that it would also be difficult to define from this observable a clear criterion that allows to decide what level of pion suppression is finally needed, different than in the case of the intermediate mass di-electrons. Therefore, we conclude that further studies on this might not absolutely be necessary for the design report. However, we will certainly follow this up in performance studies planned for the future.

Modifications:
Revision of Figs. 3.12 and 3.13
Revision of text in Sect. 3.4.1

Concerning the simulation and reconstruction procedures, they are discussed in detail and convincing evidence for the efficient electron identification is brought forward. It would be interesting if performance plots for the ordered statistics and boosted decision tree could be shown. Also, for the two methods which are described in more detail, and in particular the neural network approach, it would be interesting to give details about the foreseen training procedures to be used for real data taking.

Generally, the performance of the different electron identification algorithms is very similar. The reason for this is that the electron ID in the CBM-TRD is based on an integrated charge measurement alone and does not in addition exploit, e.g., the information on the position of the TR-photon absorption in the chambers. Due to the short drift region there is no real possibility to resolve the differences in pulse shape caused by a TR-photon and by normal energy loss, as it is possible for instance in the ALICE-TRD. Thus, all algorithms can only work on one-dimensional information. Those whose strength lies in the exploitation of correlations between two- or higher-dimensional information (e.g. between pulse height and drift time), such as ANN and BDT, therefore will not perform in any way better than those who do not use this correlations (likelihood or ordered statistics). Since the likelihood method should provide the most robust and simplest approach (also in terms of maintenance during later data analysis), we decided to use it now as the default method. As a comparison, the ANN was investigated more in detail and will be kept as an option. The other two methods (OS and BDT), however, were not investigated in further detail as soon as it became clear that they would not provide any overall

improvements. Considering the limited manpower of the project we also would prefer not to invest too much effort into this. We have added some corresponding statements to Sect. 9.3.2.

Concerning the question on reference samples needed to train the ANN, we now have added a dedicated subsection (9.3.2.5) to the text. It describes the preparation of high purity electron and pion candidates at higher momenta, not accessible with RICH and TOF, from photon-conversions and K^0_s-decays via topological cuts. This method is routinely employed for the ALICE-TRD and can also be used in the case of CBM, as demonstrated by a dedicated simulation study. For instance, one can achieve electron samples of ~99% purity this way and still is able to collect sufficient statistics to also populate the high momentum region, as needed for the TRD. These high-purity samples can then either be used to train the ANN or serve for the generation of probability density distributions, as needed for the likelihood method.

Modifications:
Revision of text in Sect. 9.3.2
Addition of subsection 9.3.2.5
Addition of Figs. 9.9, 9.10 and 9.11

Simulation

Simulations of rates, channel occupancies, radiation levels were presented, but the proper conclusions and documentation of the resulting specifications are missing in several places. In order to get a more concise idea about the integration of the TRD inside the CBM experiment, e.g. a 2D map of the radiations length and nuclear interaction length that is sitting in front of the TRD chambers would be very instructive. This should of course include the relevant support structures. A description of the interaction region will also be very useful.

We have now also summarized the main specifications on radiation levels, hit rates and occupancy in Table 2.1. The latter values naturally are taken into consideration when defining the pad plane granularity. Figs. 4.7 and 4.8 present new calculations of the detector occupancy for central Au+Au collisions at SIS100 (10AGeV) and SIS300 (30AGeV) for the updated TRD geometry, which are discussed in Sect. 4.4.1. With the new geometry and pad plane layout the occupancy is limited to maximally 5.5% at 10AGeV, which is well within specifications (< 10%). Also new trigger rate estimates are presented and discussed in Sect. 4.4.2 in relation to the requirements. On average we find 50 kHz for minimum bias Au+Au collisions at 10AGeV, with only very small regions exceeding 100 kHz.
Sect. 4.7 now also includes a 2D-map of the radiation lengths of the material in front of the TRD (Fig. 4.15). This includes all the material and support structures, as they are presently known.

Modifications:
Revision of Tab. 2.1
Revision of Figs. 4.7, 4.8, 4.9
Revision of text in Sects. 4.4 and 4.7
Addition of Fig. 4.15

Radiation levels in key areas should be tabulated, safety factors applied and the specifications for radiation tolerance for electronics components and radiation numbers for chamber ageing tests should be derived. These numbers can then also be compared to the ALICE-TRD or experience with other geometries. The overall specification of the detector has to be presented in a more clear way.

The expected radiation levels are displayed in Figs. 4.15, 4.16 and 4.17. We now also quote the numbers in summary table 2.1. However, a comparison to the ALICE-TRD, where so far no aging effects have been observed, is unfortunately not too helpful, since the so far in Run1 and Run2 accumulated radiation levels are about two orders of magnitude to the ones expected for the CBM-TRD. However, we plan to test the radiation tolerance of the CBM-TRD components also at the CERN-GIF++ facility, which should provide an environment that is at least as challenging than the one expected for CBM.

On the other side, since we use for the construction of the readout chambers only already tested and certified materials (e.g. Araldite glues, Kapton foils or G11), as they have already been used for e.g. the ALICE-TRD, no special issues on the material side are to be expected. This aspect is now discussed in a dedicated subsection (5.4.2.1).

Modifications:
Revision of Tab. 2.1
Revision of text in Sect. 4.6
Addition of subsection 5.4.2.1

Integration

The system integration of the TRD has to be worked out in more detail. E.g. the flow of Xenon through the chambers, considering height differences, gas pockets, single point failures etc. must be studied. The chamber leak rate, maximum chamber overpressure and the system aspects that ensure the protection against overpressure and loss of large amounts of Xenon must be worked out.

We now provide an upper limit on the chamber leakage rate of < 1 ml/h (see Tab. 5.1), which would result in an overall xenon loss that remains in an affordable range. However, with the ALICE-TRD a total leakage rate for the whole detector system below 20 ml/h has been achieved, i.e. a chamber leakage rate that is more than an order-of-magnitude lower than our limit. Since there are no principle differences in this respect between the situation in ALICE and CBM, we believe that a similar performance is also possible here.
As a consequence of several discussions with the expert on the ALICE-TRD gas system (C. Garabatos Cuadrado) the proposed design of the gas system has been completely revised and in many aspects even simplified. For instance, it turned out that we could safely operate with five separate circuits only. Also, the list of required components has been updated, based on the ALICE experiences.
In addition, it is planned to set up a test gas system (a very first prototype has already been operated during test beams) in order to investigate these issues in detail in the laboratory and during operation at the mCBM setup.

Modifications:
Revision of text in Sect. 8.3.2
Revision of Tabs. 8.1 and 8.2
Revision of Figs. 8.7 and 8.8
Addition of Tab. 5.1

The sensitivity of the TRD performance to pressure and temperature variations must be established. The issue of electronics cooling (air cooling vs. water cooling) must be evaluated in detail.

The sensitivity of the TRD readout chambers to pressure variation has been extensively studied, on one side with GARFIELD simulations (see Figs. 5.18 and 5.19) and on the other side by laboratory measurements (see Sect. 5.4.2.2). The main concern is that changes in the differential pressure will deform the cathode entrance window and thus modify the resulting gas gain. To limit the gain variations to a level that can be easily compensated by offline calibration procedures (i.e. below 10%) the deformation of the entrance window should be kept below ±1 mm. By supporting the entrance window foil with carbon grid structures it can be ensured that pressure variations of 1 mbar will not cause any deformations that are larger than 1 mm. Thus, the relative gas pressure (nominal value of 1 mbar) should be kept below 2 mbar for a stable operation of the TRD. This requirement is now also summarized in the Table 5.1. In addition, we now also show the sensitivity of the gas gain to temperature variations (see Fig. 5.1).

Modifications:
Addition of Sect. 5.1
Addition of Tab. 5.1
Addition of Fig. 5.1

Generally, we still believe that a system based on air cooling, potentially also including fans and heat exchangers, should be sufficient for our needs. One can compare the situation of the TRD with the one of the tracking chambers of the muon arm of ALICE. There station 5 dissipates about 2.6 kW, which can be cooled by an air flow of 600 m^3/h (quoted from the addendum to the corresponding technical design report). Assuming the same air flow, which for the TRD geometry corresponds to an air velocity of 0.32 m/s, we estimate that ~5 kW could be transported outside of the gap between the TRD layers which is close to our current estimate of 4.6 kW per layer (the expected heat dissipation has been updated based on recent measurements and also taking the DC-DC converters into account). Using fans and heat exchangers the air flow could in principle easily be increased even further. However, it also needs to be assured that no local hot spots and

too steep temperature gradients are produced. Furthermore, it has to be investigated whether special cooling bodies are needed to transfer the heat from the electronic components to the flowing air. To study this in detail in a realistic environment, we plan to construct a dedicated detector mock-up. This will be put together from real readout chamber prototypes and electronics, plus additional adjustable heat sources (resistors), in the same geometrical configuration as for the real detector. With this setup a detailed study of the cooling concept can be performed. In the case that it turns out that for the innermost part of the detector air cooling is not sufficient, we would foresee the installation of a water cooling system here.
The text in the TDR has been updated to describe the situation more in detail.

Modifications:
Revision of text in Sect. 8.6
Revision of Tabs. 8.4 and 8.5
Revision of Fig. 8.10

The global support structure and fixation of the chambers on this structure also has to be presented in to sufficient detail.

A new design of the support structure is now presented in the design report together with the details of the chamber fixation, as we currently foresee it. These are based on aluminum profiles, whose cross section has been minimized to achieve a small material budget without compromising the stability. However, some parts of the structure can optionally be replaced by carbon sheets in order to further reduce the material budget even further. We are currently constructing a test setup for the support structure in the laboratory, which will allow to evaluate these possibilities and the fixation of the chambers in detail in a realistic environment and to study the mechanical stress distributions. The results of its evaluation will determine the final layout of the support structure in the coming year.

Modifications:
Revision of text in Sect. 8.2
Revision Figs. 8.2 and 8.3
Addition of Fig. 8.4

It seems that the radiator is operated in the 'cavern atmosphere'. Are there issues related to this? What are the specifications on the cavern environment with respect to temperature and humidity?

The radiator will in fact be operated in the cavern atmosphere in the same way as the one for the ALICE-TRD. We do not plan to operate it in a specially controlled atmosphere (e.g. nitrogen). However, it is foreseen to encase the main active radiator material, i.e. the foam foil layers, in a box composed of hard foam (PMMA or PE hard foam). This box will surround the foils on all sides except the one facing the entrance window of the readout chamber. This side will instead be closed by the outermost radiator foil itself, which will be glued in an airtight manner to the radiator box. Thus, the radiator material should quite effectively be shielded from changes in the ambient atmosphere and other external influences. Also, a potential leakage of xenon into the radiator would be prevented this way. Therefore we do not expect any severe problems with external influences to the radiator and also have up-to-now not experienced any in our test beam campaigns.

Modifications:
Revision of text in subsections 6.3.1 and 6.3.2
Addition of Figs. 6.8 and 6.9

An overall idea for the detector control system should also be presented, e.g. where will temperature sensors be placed, will the DCS operate through the GBT or is it an independent system through e.g. Ethernet that does not rely on the readout system being operational etc.

We have extended the section on DCS. The system naturally should operate independently from the GBT-based data readout for safety reason. It is foreseen to use DCS boards communicating via Ethernet to monitor and control the relevant detector parameters. The foreseen sensors, their positions and the parameters to be controlled are now summarized in a dedicated table (Tab. 8.9).

Modifications:
Revision of text in Sect. 8.7
Addition of Tab. 8.9

Chambers and test beam

Some details on the HV system should be presented in terms of number of wire groups connected together, the estimated capacitance for one wire group, the choice for the value of the decoupling capacitor, the type and reliability of the decoupling capacitor.

We intent to group the anode wires into maximally nine HV segments which will be decoupled via the HV filter board. One segment in this case will thus contain around 24 anode wires in case of the small and 44 for the large modules, resulting in capacities of 74.2 pF, resp. 242.0 pF. The decoupling capacitor is planned to be identical to the one used already for the ALICE-TRD and has a value of 2.2 nF. These values are now also quoted in the text. Naturally, these elements need to be carefully tested before installation, but the capacitors performed very well for the ALICE-TRD over the whole time the detector is operational. Also, we extensively used them already in several test beams with large CBM-TRD prototypes without any problems.

Modifications:
Revision of text in Sect. 8.5

The overall calibration strategy for the wire chambers should be discussed. The operation point also has to be defined properly, sensitivity to temperature and pressure variations, the nominal operating gas gain, the specified noise in terms of ADC counts, the ADC bin position where the MIP peak is placed, what is the dynamic range with …

The main parameters concerning the chamber operation are now defined in Tab. 5.1. It specifies the required signal-to-noise ration, the MIP peak position and the gas gain, along with other relevant parameters such as the applied voltages in the case of argon and xenon operation. We also now discuss in Sect. 5.1 the corresponding requirements concerning stability (e.g. gas temperature and pressure), supported by additional GARFIELD simulations (Fig. 5.1).

Modifications:
Revision of text in Sect. 5.1
Addition of Tab. 5.1
Addition of Fig. 5.1

3 types of FE boards and 3 types of RO boards were presented, with the prospect of reducing to 2 types of FE boards and just one type of RO board. Clearly it is strongly recommended to aim for the smallest possible number of board types.

We have performed an extensive re-evaluation of the overall TRD geometry. The main aim was on one side to reduce the number of different TRD modules, as well as FEB types, needed to compose the overall detector. On the other side it was attempted to optimize the usage of the e-links for a maximal efficiency and thus reduced cost. For this purpose several new geometries were designed and extensively evaluated in simulations in order to ensure that it provides an optimal performance for reconstruction and in particular particle identification. One important aspect in this evaluation was the question what maximal pad sizes can be afforded without compromising the ability to assign found hits to tracks in a unique way. I.e. the number of fake hits and of hits that are distorted by signals from different particles should be kept minimal to ensure an accurate and unambiguous determination of the energy deposition in the chamber gas. Also, large pad sizes will have disadvantages in terms of the measurable signal-to-noise ratio.
As a result of the exercise, we concluded that a geometry based on only four different module types will provide the same performance than the original version composed of six different types. The new arrangement will have two different large types in the outer wings of the setup, while the central stack will be composed of two different small module types. This configuration also greatly simplifies the construction of the support structure, as well as the routing of the service lines. It only needs four different types of front-end boards and will make an efficient use of the necessary GBTx-links (the resulting e-link efficiency would be ~90%). The pad size, which is largest in the outer large chambers, is limited to 8cm^2 in the final version of the geometry in

order to keep the distortions of the charge measurements at a minimal level also in high multiplicity events. Also, this avoids issues with low signal-to-noise ratios due to too large pad capacitances.

Modifications:
Revision of text in Sects. 4.2, 5.5 and 7.2
Revision of Figs. 4.2, 4.7, 4.8, 4.9, 4.16, 5.21, 5.22, 5.23, 8.2 and 8.11
Revision of Tabs. 4.1, 5.2, 5.4, 5.5 and 7.7

The pad planes and the signal connectors do not contain any ground connections, all the grounding of the FE board and readout board is referred to the aluminum chamber structure. The electrical scheme for this overall system should be presented and discussed in some detail.

Generally, the grounding scheme follows the one implemented for the ALICE-TRD, i.e. no direct ground connections to the pad plane and signal connectors are foreseen. During the operation of the ALICE-TRD no problems were experienced with this grounding scheme and we thus would also not expect any in case of the CBM-TRD. Also, adding individual ground connections to the connectors would dramatically increase their complexity and it would be difficult to find appropriate commercially available types.

The results of the large-scale test beam together with other CBM subsystems are of course important steps, they should however not replace tests that are dedicated and optimized for very chamber specific tests. E.g. a test at the GIF++ that should simulate the performance under global chamber illumination at realistic rates is very important. A setup to assess position resolution in a better way will also be helpful.

We agree that chamber specific tests need to be continued. A first test at the GIF++ facility was performed in October 2017 in order to study the behaviour of the readout chambers under very high loads. First estimates indicate that the charged particle rates, generated by electrons produced by Compton-scattered photons provided by this facility, are similar, or do even exceed, the ones to be expected during CBM operation. During the test at GIF++ we did not experience any immediate problems in operating the readout chambers and front-end electronic under this extreme environment. The detailed analysis of the data is currently on the way and relevant results might still be added to the TDR as soon as they become available.
Another additional test beam was done in September 2017 at DESY in Hamburg. Here electron beams can be provided with momenta between 1 and 5 GeV/c. These data will be used for a detailed and systematic performance study of radiators and the detector response. The measured spectra will serve as a comparison baseline for our detector simulation and will help in further refinements of the digitization part of the TRD simulation. Also, further measurements of the position resolution were done in the clean environment at DESY. The analysis of the DESY data has just been started and relevant results might also still be added to the TDR, if required.
The measurements from previous test beam campaigns were unfortunately somewhat hampered by the fact that no reference detectors with adequate precision were available within the new FLES based readout scheme. The analysis of the data from the CERN-PS using scintillating fiber hodoscopes as reference detectors however agrees very well with the expected position resolution of 300 µm after correction for multiple scattering (see Sect. 4.5.2). Also, the pad response function extracted from the data is very close to the theoretical expectation. Therefore, we believe that the proposed MWPC design is performing according to specifications.

Modifications:
Revision of text in Sect. 4.5

The detector performance in terms of resolution and rejection power should be compared to simulations and be properly implemented in the overall CBM simulation in order to guarantee consistent performance studies.

Generally, we believe that the detail of simulation is currently on a relatively high level and adequate for the ongoing performance studies. As described in chapter 5, the geometry is implemented in the Geant part on a quite detailed level and is also now including a description of the support structures and services. Chapter 9 describes the detector simulation (i.e. digitization), which uses the energy in the readout chamber gas volume as determined by Geant as input and calculates the charge induced on the pads according to a realistic pad response function. Therefore, the simulated point resolution should be very close to the real situation (see also Fig. 9.12). The simulation of the charged release via energy loss in the xenon gas and the absorption of transition radiation are implemented in the Geant part in the same fashion as used for the ALICE-TRD. Since Geant3 cannot handle the latter in a satisfactory manner, we use a momentum dependent parameterization of the produced TR spectra and a realistic absorption spectrum for the gas (see the discussion in chapter 6). This has been tuned to match the measured performance of the radiator types K++ and N25 (see Fig. 9.3) and should thus give a good description of the overall performance. In fact, we expect the radiator H, which is our default solution, to be even superior, such that the current simulations can be considered as being conservative in terms of pion rejection.
Overall, we consider the current implementation of the TRD as being sufficient for the performance studies that are shown in the technical design report. Of course, in a next step we aim at detailed improvements, both in the description of detector geometry and of its response. The latter will be extended by a detailed model of the electronics response (including e.g. shaping, cross talk, noise, etc.), which will improve the simulation even further. However, judging from previous experiences the differences (e.g. ALICE-TRD) will only be minor and should not affect the overall performance. Furthermore, it is planned to gauge the simulation results with dedicated test beam data, which were collected in Sept. 2017 at DESY. The data allows extracting detailed detector responses at various beam momenta, which can then directly be compared to the corresponding simulated responses. This procedure will help to further improve the simulation.

Modifications:
Revision of text in subsection 6.3.1

The test under full illumination is also important to verify that the system of triggering neighboring channels for the readout, either on the same chip or even on the neighboring chip, does still operate properly in an environment with a large overlap of 'self triggering' and 'neighbor triggering' channels and the system shows 'graceful degradation' when put to rates beyond the nominal ones.

The total data rate of SPADIC is limited by the two data output links, which can transport a payload of roughly 10.6×10^6 frames/second (per link). The data volume required for one hit has been optimized in SPADIC2.1, where only 2 frames are required (providing 3 data samples). Data volume obviously increases, if more samples are read per hit, for instance to 4 frames for 8 samples.
A hit in one channel only gets lost when the local FIFO (64 frames depth) is 'almost-full', because the overall chip data rate is approaching the maximum. In such a case, an error message reporting about the FIFO-full condition is written to the FIFO (the 'almost-full' condition is set such that this error message still fits). Further events with blocked FIFO are counted in each channel, until the FIFO is ready again to take data. At that point a message reporting about the number of lost hits is first written to the FIFO, and normal operation is resumed.
To summarize: Short-term fluctuations in the distributed data rate are buffered by local FIFOs. Larger / longer fluctuations can block channels for a limited time, but the occurrence of this situation is flagged and the number of lost events is reported. Significant losses occur when the total chip rate approaches the output data rate limit.

Electronics

The reviewer comments were very valuable to help better understand the ASIC and improve our design. An improved ASIC version, SPADIC2.1, has been submitted on 24.7.2017, incorporating several suggestions.

Modifications:
Revision of text in Sect. 7.1
Revision of Tabs. 7.2 and 7.3

For the SPADIC specification, a Qmax of 75fC is quoted. The full linear range of the analog fronted should be measured and presented.

SPADIC2.1 has two selectable gain settings, 'low gain' and 'high gain', which differ by a factor 2. The simulations below show the shaper output for input charges of 0 to 100 fC in 10 fC steps for both cases. As it can be seen, the 'low gain' mode is linear up to nearly 100 fC.
Measurements on SPADIC2.0 are presently being set up and results will be ready soon.

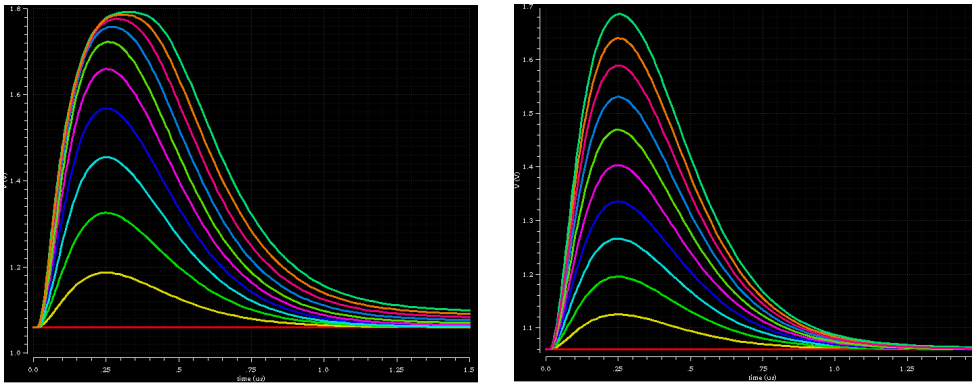

Simulated SPADIC2.1 shaper output for charge injections of 0 … 100 fC in 10 fC steps. The left simulation shows the 'high gain' setting, the right the 'low gain'.

The reaction of the frontend to highly ionizing events of 10, 100, 1000x the average charge should be measured and studied. The recovery time of the shaper output is one measure of the related dead time. By injecting a sequence of very large and small pulses one can assess whether the preamp shows saturation and dead time that would not be visible at the shaper output.

SPADIC2.1 includes a nonlinear element in the feedback path of the preamplifier to discharge the input node faster for large charges compared to the normal feedback path. The simulation below shows the responses of preamplifier and shaper to an 'overload' charge of 10/100/1000/10000 fC followed after 7 µs by a normal signal of 10 fC. This shows that the simulated overload recovery time is in the order of 5 microseconds. Note that this time depends on the various bias settings, in particular the CSA feedback current.
Measurements on SPADIC2.0 are presently being set up and results will be ready soon.

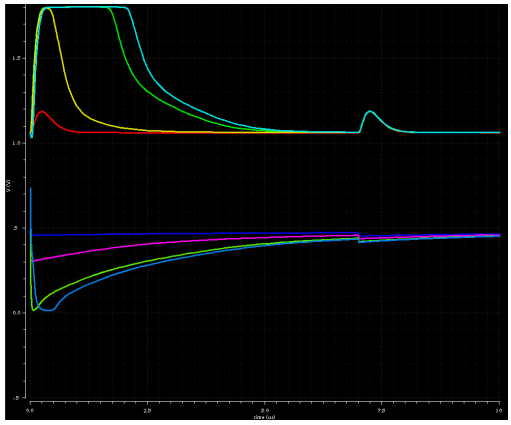

Simulated response of Charge Amplifier (bottom) and shaper (top) for a large 'overload' charge of 10/100/100/10000 fC followed by a 10 fC signals.

It should also be verified whether the preamp/shaper stays in the operational regime for the effective persistent input current represented by the actual charge that is flowing onto the readout pad. This situation can be easily overlooked in lab tests and test beams with short spills.

The chip is intended for readout of an isolated cathode electrode so that no significant leakage currents are expected. No special measures have been taken in the chip to sink leakage, so that any leakage leads to a DC shift in the preamplifier and shaper signals. This is illustrated in the simulation below, where preamplifier and shaper output for a 10 fQ charge signals are shown for 0 and 2 nA of leakage current. The shift introduced by the 2 nA DC current corresponds to roughly 10 fQ of charge. This shift depends strongly on the setting of the feedback resistor bias in the CSA.
Measurements on SPADIC2.0 are presently being set up and results will be ready soon.

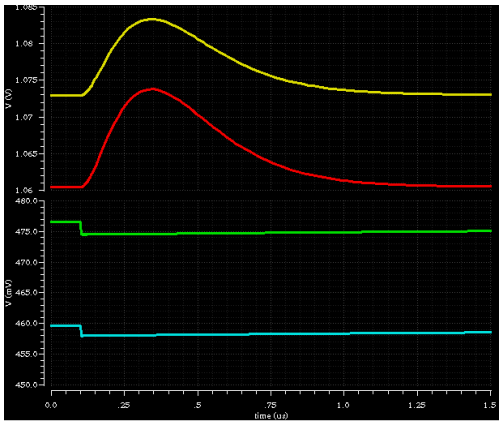

Preamplifier (bottom) and shaper output (top) for a 10 fQ charge for no and 2 nA leakage current.

The radiation requirement including safety factors should be specified and related to the used technology. Are radiation tests to the expected levels planned for TID and 1MeVneq fluence?

Concerning TID tolerance, we rely on the intrinsic properties of the UMC 180nm technology used. This technology is also used in projects with larger exposure levels. X-Ray irradiations of a very similar chip (DCD for Belle containing very similar ADCs) to levels > 7 MRad have been carried out without visible degradation. We believe the effects of TID have been well understood and further tests are therefore not required. We presently do not plan for TID tests with SPADIC.

Concerning single event effects, we have implemented the following approach in SPADIC2.1: All static configuration data in the analogue (584 bits) and the digital (117 registers of 15 bits) parts is connected in a long 'XOR-chain' to form a one bit parity signal of all bits. This signal can be monitored via slow control read accesses. Whenever a (single) bit flip occurs, configuration data will be re-written, which takes about 100 µs and can be done in parallel to data acquisition. No protection has been included on state machines, but all state machines come back to valid states in case of upsets, so that 'hang-ups' are avoided. The occurrence of single event upsets will be monitored anyway in all chip operations. A dedicated SEU test campaign is not planned, but we could participate parasitically at other campaigns, e.g. at GIF++.

The specification of the shaping time with respect to both, Argon and Xenon, operation should be discussed.

The peaking time of the shaper signals can be changed fairly easily by exchanging passive components (Rs and Cs). This has been exercised already when moving from SPADIC1.0 (80 ns) to SPADIC2.0 (245 ns). SPADIC2.1 has a design CR-RC peaking time of 120 ns. It can be switched to a CR-$(RC)^2$ shaping with a peaking time of 240 ns, as shown in the simulation below. The ASIC designers are prepared to adjust the final shaping to the value fixed by detector scientists.

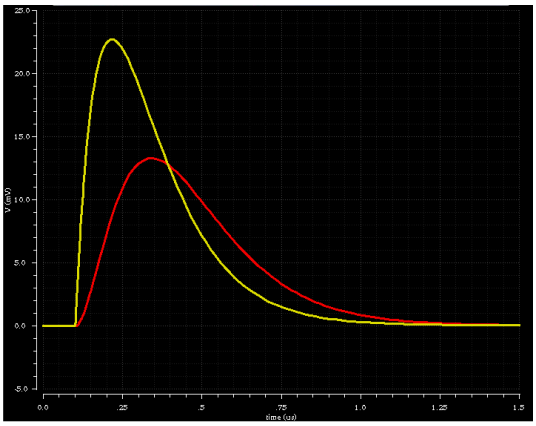

Simulated shaper outputs for the 'fast' and 'slow' settings: The 'fast' setting uses CR-RC shaping with a peaking time of 120 ns. The 'slow' settings adds a further RC stage so that a CR-$(RC)^2$ shaping with a peaking time of 240 ns is obtained.

For commissioning and calibration purposes it would be extremely useful to have a mode that allows the readout of a continuous sampling of the baseline for the individual channels on the chip (of course not at the same time).

The shaper output of any channel can be monitored by force-triggering an event with a digital message. The pulse-pick pattern can be set to its maximum, so that 32 consecutive samples are sent out. A further force-trigger before the end of this pulse train leads to a seamless extension of the sample data stream. A continuous data stream is therefore possible by force-triggering a channel with a high enough rate (which is possible via the down-link: One force trigger can be sent every 10 samples).

The baseline correction is now postponed to the FPGA (Feature Extraction). However much more information about the baseline is available in the SPADIC chip itself. Please consider as option (which can be turned off) a simple baseline correction circuit in the SPADIC 2.1, e.g. like in the TRAP chip.

The baseline of a hit is best determined through samples occurring before the actual hit starts. This is possible using so-called 'pre-samples', which can be selected as part of the normal pulse-pick pattern. Up to 3 pre-samples are possible in SPADIC2.1.
A more sophisticated estimation of the baseline can be obtained by averaging the channel sample data continuously. This feature suggested in the review has been implemented in SPADIC2.1. Detected pulses are excluded from the averaging process. The average baseline can be chosen instead of a pre-sample. Furthermore, the digital IIR filter can be used to attenuate fluctuations in the baseline.

It also has to be guaranteed that a single noisy channel on the chip does not fully occupy the output buffers. Can an individual noisy FE channel be switched off? Clock gating of the unused digital filter stages could save power.

Each channel can be disabled digitally. All signals communicating with the rest of the chip are set to their inactive state. Furthermore, the clock in the digital section allocated to the channel is turned off to reduce power consumption.

A global power-down pin has been added to SPADIC2.1. It sets the consumption of the analogue part to zero, irrespective of bias DAC settings. The Bias DACs can then be set to reasonable values, before the analogue parts are activated by releasing the power-down pin.

Decision on alternative solutions

Assuming an optimistic TDR timeline with approval by the end of 2017, the milestones as presented to the referees are not maintainable. Engineering Design Reviews and Production Readiness Reviews have to be included in the list of milestones. System developments and final design considerations for EDR and PRR typically take at least one year, which will move start of production to 31.12.2018 at best.

The milestones given in 11.3.1 have been reassessed and updated. We now include an additional time period until mid-2018 for the preparation of EDR and PPR and consequently the start of production has been shifted.
We have also updated the tables with the cost estimates. In particular, we now include contingencies (e.g. production of spare readout chambers) and more realistic numbers for the gas system and cabling.

Modifications:
Revision of text and tables in subsections 11.2.1, 11.2.2 and 11.3.

The alternative chamber design is certainly very elegant and innovative, and the level of evaluation and tests is very impressive. The performance of the alternative electronics is also demonstrated to work well, it is however not yet on a level that is integrated in the system – digitization and readout logic development are still ahead which takes significant time and effort.

Unless a significant improvement in overall performance for the CBM physics program can be demonstrated for the alternative solutions, the referees recommend to base the project on a uniform system using the presented baseline. In view of the presented timeline, the time for a decision has long passed and all efforts must now be focused on the development of the system aspects of the TRD project.

We agree with the notion that, considering the time scale of the project, a decision on the overall system design should be made very soon. In fact, we are currently convinced that the baseline design, as described in the current design report, meets all the performance requirements, which are posed to the TRD for an operation at SIS100, and will provide the fasted path towards a working detector system.
However, as one possible alternative option we are currently still assessing the readout chambers with a triangular pad layout, which intrinsically provides a better position resolution. This design is currently being implemented in the simulation geometry and into the digitization procedure. Based on this performance studies will be done, in order to assess whether this solution provides significant advantages compared to the baseline layout which outweigh the increase in complexity, e.g. a better tracking performance or allowing for the same physics performance with fewer detector layers. These points will be investigated in a separate document as an addendum to the current design report. If this solution turns out to provide significant advantages in this respect, we would still consider this version for the inner zones of the detector. Our current installation sequence foresees to begin the installation with the large modules in the outer two segments and to end with the small modules in the inner regions. Therefore, there should be time enough for this evaluation and a decision on the design of the inner modules could await the readiness of the addendum.

Modifications:
Removal of Chap. 12.